European Drag Reduction and Flow Control Meeting – EDRFCM 2015
March 23–26, 2015, Cambridge, UK

Control Mechanism of DBD Plasma Actuator for Deep-stall Flow around NACA0015 at $\mathbf{Re} = 6.3 \times 10^4$

H. Kato
Department of Engineering, University of Tokyo, Sagamihara, Kanagawa, 252-5210, Japan

M. Sato, H. Aono, A. Yakeno, K. Fujii
Institute of Space and Astronautics Science, JAXA, Sagamihara, Kanagawa, 252-5210, Japan

INTRODUCTION

In the past decade, one, Active Flow Control (AFC) have attracted the significant attention in the world. In AFC research, dielectric barrier discharge (DBD) plasma actuators (PA) have been widely researched, because of their high responsiveness, flexibility of implementation into existing designs and low energy consumption (Fig 1). For separation control around airfoils at low-middle Reynolds numbers （$\sim 1.0 \times 10^6$） , many computational and experimental studies have shown the applicability of PA. In this condition, it has been found that using an unsteady input voltage “burst mode (Fig 1)” gives a better separation control capability than continuous input voltage. This control capability of burst mode has been shown in other AFC (synthetic jet, control plate).

The control mechanism (Fig 2) of burst mode is classified at low Reynolds number （$O(\sim 10^4)$） . Previous work [1] has shown that the flow control mechanism is assumed to be equivalent to how the momentum is provided in the bottom of boundary layer to overcome the adverse pressure gradient. In this viewpoint, the mechanism is firstly characterized into 1)direct momentum addition and 2)freestream momentum induction. The burst mode effectively uses mechanism 2). This mechanism 2) is subdivided into two items: 2-i)use of (two-dimensional) large-scale(organized) vortex and 2-ii)use of turbulent vortices. It is proposed that in terms of Reynolds stress, mechanism 2-ii) is more important for flow control around airfoil at near stall angle. Still at higher angle of attack, there are few guidelines which mechanism 2-i) or 2-ii) is more important to enhance the controllability of PA.

In this research, we focused on flow control of deep stall, and discussed more important control mechanism. For this purpose, Large-eddy simulations on the separation control by PA around NACA0015 were conducted. With these results, we clarified that mechanism 2-i)use of large-scale vortex is more important to control the separation of deep-stall.

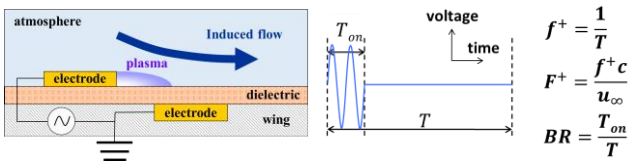

Figure 1: Configuration of the DBD plasma actuator and Burst mode image.

1).Direct momentum addition
2).Free stream momentum induction
2-i).Use of large-scale vortex
2-ii).Use of turbulent vortex
2-ii-A).Transition to turbulent
2-ii-B).Enhancement of turbulent intensity

Figure 2: Classification of the mechanism of control of separated flow [1].

NUMERICAl METHOD

LANDS3D[2] was employed for all LES simulations. Table1.shows computational methods. The zonal method is employed to treat the region of small body force. Figure 3 shows the computational grids. The grids for LES consist of two parts: an airfoil blue grid (zone 1); and a fine red grid (zone 2).

Table 1: Computational methods.

governing eq.	Compressible Navier-Stokes equations
spatial derivatives	6th-order compact difference scheme
filtering	10th-order filtering
time integration	backward 2nd-order difference ADI-SGS
SGS model	N/A(low-pass filtering)

The body force by Suzen model [3] is used to simulate the effect of PA. The unsteadiness of body force according to the AC frequency is represented as follwos:
In all control cases, momentum coefficients(C_μ) of body force is set to $C_\mu = 8.24 \sim 65.92 \times 10^{-5}$. This value correspond to maximum plasma induced flow velocity ($u_{jmax}/U_\infty = 0.7$). Table 2 shows the computational parameters of each case.

Table 2: Computational cases.

Case name	*Location*[%]	*fbase* [Hz]	F^+	$BR\,[T_{on}/T]$	u_{jmax}/U_∞	$C_\mu \times 10^{-5}$
OFF	N/A	N/A	N/A	N/A	N/A	N/A
BR 0.1	0	6000	6	0.1	0.7	8.24
BR 0.8	0	6000	6	0.8	0.7	65.92

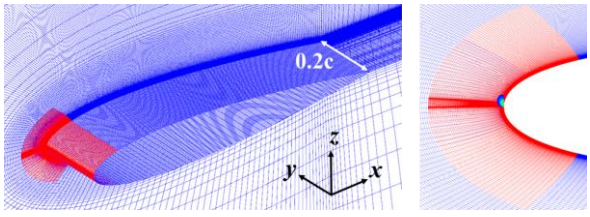

Figure 3: Computational grids.

RESULT

Fig 4 shows the distributions of the time-averaged($t^* = 4\sim16$) chordwise velocity. In terms of the distributions of time-averaged chordwise velocity, the separation is suppressed to some extend for BR0.1 case. On the other hand, the separation is clearly suppressed for BR0.8 case.

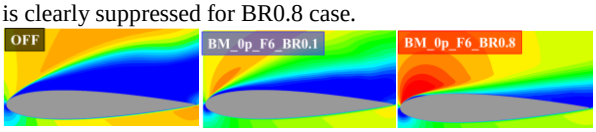

Figure 4: Time-averaged flow field of the x-direction velocity u/U_∞ (averaged in $4 \leq tU_\infty/c \leq 16$)

However, for BR0.1 case separation is suppressed temporarily like BR0.8 case focusing on instantaneous flow-field. Fig 5 shows the time-history of Drag coefficient (C_D). From Fig 5, almost the same aerodynamic performance appears to both BR0.1 and BR0.8 cases during $t^* = 4\sim10$ (control-phase).

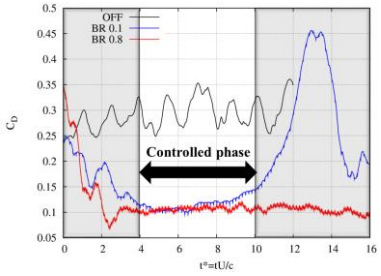

Figure 5: Time-history of Drag coefficient C_D

Therefore in the following analysis, the control mechanisms 2-i) and 2-ii) in the control-phase are focused on. Fig 6 shows time-averaged in control-phase flow-fields. For BR0.1 and BR0.8, the separation is clearly suppressed in control-phase.

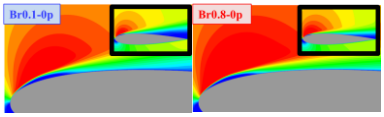

Figure 6: Time-averaged flow field of the x-direction velocity u/U_∞ (averaged in $4 \leq tU_\infty/c \leq 10$)

2-ii)the rapidity of the turbulent transition is evaluated quantitatively. Fig 7 shows TKE maximum value in the wall-normal direction is plotted against the chord direction. From previous work about the laminar-turbulent transition of free shear flows [4], the fluctuation of flow direction velocity increases gradually and decrease after a peak. Based on the above knowledge, the peak of turbulent kinetic energy (TKE) is considered transition point. Fig 6 shows that there is no difference of the transition point and rapidity among BR0.1 and BR0.8. In other word, there is no difference in the mechanism 2-ii) among BR0.1 and BR0.8.

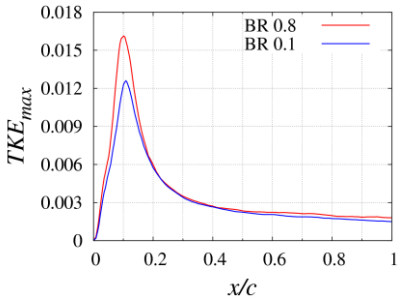

Figure 7: TKE maximum value distributions.

2-i)large-scale vortex is evaluated qualitatively. Fig 8 shows phase-averaged contour lines of second invariant of velocity gradient tensor over periodic components of Reynolds stress of each phase. Comparing two control cases, BR0.8 case's Reynolds stress around large-scale vortex is stronger than Br0.1 case's. Although the detailed reason is unclear, high burst ratio leads to stronger vortex and maintains flow reattachment. Fig 9 shows pressure coefficients (C_p) on the airfoil surface of each phase. From pressure coefficients, large-scale vortex shedding is captured as small peak from 5% to 60% of the chord length in BR0.8 case.

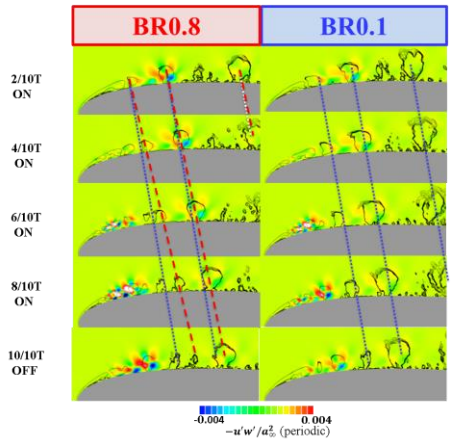

Figure 8: Periodic components of Reynolds stress of each phase

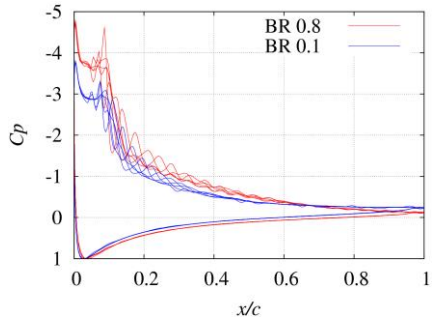

Figure 9: Pressure coefficients on the airfoil surface of each phase

CONCLUSIONS

LES showed that 2-i)use of large-scale vortex is more important control mechanism in the deep stall control.

REFERENCES

[1] Nonomura, T., Aono, H., Sato, M., Yakeno, A.,Okada, K., Abe, Y., and Fujii, K., "Control Mechanism of Plasma Actuator for Separated Flow around NACA0015 at Reynolds Number 63,000 –Separation Bubble Related Mechanisms-," *AIAA 2013-0853*, 2013.

[2] Fujii, K., "Developing an Accurate and Efficient Method Based on the Fortified Solution Algorithm," *Journal of Computational Physics*, vol. 118, 1995, pp.92-108.

[3] Suzen, Y. B. and Huang, P. G., "Simulation of flow separation control using plasma actuator," *AIAA Paper 2006-877*, 2006.

[4] Sato, H. and Saito, H., "Fine-structure of energy spectra of velocity fluctuations in the transient region of a two-dimensional wake," Journal of Fluid Mechanics., Vol. 67, 1975, pp.539-559.